Improved Recyclability of Cast Al-Alloys by Engineering β-$Al_9Fe_2Si_2$ Phase

C.B. Basak and N. Hari Babu

Abstract

Castability and tensile properties of recycled cast Al–Si alloys are affected by the presence of high iron content. The present study demonstrates a promising scope of better recyclability by engineering the intermetallic β-phase that present in cast Al–6 wt%Si model alloy systems with as high as 2 wt%Fe. Thermodynamic interplay between Si and Fe concentration on the formation of the β-phase and the solidification behaviour of this hypoeutectic Al–Si alloy has been explored. It has been demonstrated that suitable heat treatment alters the morphology of the β-phase and simultaneous addition of Cu improves the strength. Based on the experimental evidences, the mechanism behind the solid-state morphological changes of beta phase has been proposed. Experimental results and thermodynamic calculations suggest that Cu content of more than 2 wt% marginally increases the yield of beta phase; however, at 4 wt%Cu the solid solution strengthening improve the strength of solutionized alloy.

Keywords

Aluminium alloy • Intermetallics • Precipitation • Thermodynamic modelling • Scanning electron microscopy

Introduction

Primary production of aluminium from bauxite ore attracts an energy expenditure of about 186 MJ/kg of metallic aluminium; however, this expenditure could be reduced to 10–20 MJ/kg by recycling the discarded aluminium products or scraps [1, 2]. These figures emphasize not only the economic importance but also the underlying environmental benefits in the favour of recycling aluminium scraps. Recyclable scrap may come from manufacturing industries, automobile sector, beverage cans and from other miscellaneous sources. Because of the diversified sources and involvement of processing equipment the recycled aluminium accumulates several metallic impurities, e.g. Si, Mg, Ni, Zn, Pb, Cr, Fe, Cu, V, Mn to name a few. Different physical separation techniques are being employed in the industries today before melting the Al-scraps to minimize the impurity pick up in the recycled aluminium products; e.g. magnetic separation, air separation, heavy media separation (using water based slurry) and colour sorting [3]. Despite employing such physical separation techniques, iron pick up from the handling and processing equipment remains inevitable. This residual iron impurity poses as the major challenge for the recycled aluminium because of two main reasons. Firstly, higher iron content usually associated with less flowability and shrinkage porosities in the casting, i.e. poor castability and secondly, it drastically reduces the ductility due to the formation of intermetallic phases, specifically the β-phase.

Al–Si alloys are usually considered as cast alloys and have applications in automobile sectors. Higher iron content in Al–Si alloy system causes formation of several intermetallic phases, e.g. hexagonal α-Al_8Fe_2Si (τ_5), monoclinic β-$Al_9Fe_2Si_2$ (τ_6), δ-Al_4Fe_2Si (τ_{11}) etc. along with other

C.B. Basak (✉) · N. Hari Babu
BCAST, Brunel University London, Kingston Lane, Uxbridge, Middlesex UB8 3PH, UK
e-mail: chandrabhanu.basak@brunel.ac.uk

A.P. Ratvik (ed.), *Light Metals 2017*, The Minerals, Metals & Materials Series,
DOI 10.1007/978-3-319-51541-0_137

binary Al–Fe compounds ($Al_{13}Fe_4$, Al_5Fe_2 etc.); further details on these intermetallic compounds are available in the literature [4–7]. However, thermodynamic selection of intermetallic phase formation is strongly dependent on the concentration of both Fe and Si [8, 9].

The room temperature intermetallic phase in high Fe containing Al–Si alloy is the so-called β-$Al_9Fe_2Si_2$ phase, also designated as β-Al_5FeSi or τ_6 phase as reported in the literature [4–9]. It is known that this inherently brittle β-phase is formed as three-dimensionally interlinked thin platelets with characteristic needle-like appearance [10, 11]. This interconnectivity of the β-phase along with its poor thermal conductivity causes retention of isolated liquid metal pool in the inter-dendritic cavities causing shrinkage porosity in the final casting upon solidification [12]. Higher Fe content in the Al–Si alloys also causes reduced fluidity of the molten alloy causing inefficient and rather poor die filling [13]. These factors together render poor castability in high-Fe Al–Si alloys as mentioned earlier. On the other hand, the sharp corners (and often incoherent interface) of the β-phase act as stress raisers in the matrix causing severe brittleness in the final casting; with a comparatively lower strength and no more than about 3% ductility [9]. The only apparent advantage of having higher Fe content (up to about 0.9 wt%Fe) is the avoidance of die sticking or soldering in the die castable Al–Si–Fe alloys [10].

The most straightforward approach to counter the level of iron impurity is to dilute the recycled aluminium using primary aluminium, also known as "down cycling" [3]. A second approach is to hinder the formation of β-phase by Mn addition, in case of moderate Fe level, by promoting the formation of $Al_{15}(Fe, Mn)_3Si_2$ phase having polygonal morphology. Such change in morphology actually improves the ductility of the castings. However, beyond about 1.2 wt %Fe both needle like β-phase and polygonal $Al_{15}(Fe, Mn)_3Si_2$ phase appears which diminishes the positive effect of Mn addition [12]. The question we address in this paper is, if recycled Al-Si cast alloys can accommodate more than 1.2 wt%Fe concentration without Mn addition.

In Al–Si alloys almost all Fe contributes to the formation of equilibrium β-phase (i.e. higher Fe causes more phase fraction of β-phase) owing to its extremely low solid solubility in Al of about 10 ppm [14]. Therefore, it makes sense, rather than focusing on Fe, to focus on dealing with the β-phase. This approach could offer an indirect way to deal with the high Fe content in Al–Si alloys. Two different methodologies could be proposed based on this philosophy; namely, gravitational segregation of β-phase and alteration of morphology of the β-phase; which has been discussed in details in the literature [9]. It suffices here to state that the segregation of β-phase in liquid alloy is possible owing to the difference in the density between the β-phase and liquid-Al. However, we note that segregation of β-phase changes the overall chemistry of the liquid alloy towards low iron as well as low silicon content; whereas alteration of morphology of the β-phase targets to keep the chemistry invariant and yet tries to improve the mechanical properties. Segregation of β-phase can only take place before the final casting is produced; whereas altering the morphology of β-phase can be done in the final cast product using suitable heat-treatment. Along the similar line of thought, one could use filtration technique as well to separate the β-phase from the molten liquid [15].

Experimental Procedure

Al–6 wt%Si–2 wt%Fe was chosen as the model alloy; for the sake of brevity this alloy would be referred as 6Si alloy or base alloy in the rest of the article. Also, 2 and 4 wt%Cu was added to see the effect of Cu in the tensile strength of the alloy under different heat treated condition. Al ingots, Al–50 wt%Si, Al–45 wt%Fe and Al–40 wt%Cu master alloys having commercial purity level were used for preparing the alloy. A resistance furnace and boron nitride coated clay bonded graphite crucible was used for preparing the alloy. First Al ingot was melted and then Al–Si and Al–Fe master alloy was added sequentially with stirring. A melt of about 1 kg was prepared at 800 °C with intermittent stirring of at least 6 times with a total holding time of 2 h to ensure chemical homogeneity. Commercially available degassing tablet was used and the top oxide layer of the melt was skimmed off. Finally, the melt at a temperature of 750 °C was poured into a boron nitride coated mild steel rectangular block preheated at 250 °C. An average cooling rate of about 4–5 °C/s was expected based on previous experiments and existing literature [8]. A part of the melt also poured in a 60 mm dia. steel die for chemical analysis using glow discharge optical emission spectroscopy (GD-OES). GD-OES chemical analysis is provided at Table 1, which is averaged over five analyses from five random locations.

For microstructural analysis, standard metallographic practice was adopted where final polishing was carried out using 0.25 μm colloidal silica. An aqueous solution of 10 wt%NaOH was used for chemical etching, whenever required. A field emission scanning electron microscope (FESEM) (having both secondary electron (SE) and back scattered electron (BSE) detectors) equipped with energy dispersive spectroscope (EDS) was used for microstructural analysis. An x-ray diffractometer was equipped with solid-state detector and operated at 1.6 kW Cu–K_α radiation. Thermodynamic calculations were performed with CALculation of PHAse Diagram (CALPHAD) methodology using PandaT software [16] and image analysis were carried out using ImageJ software [17]. Tensile testing was carried out in selected specimens with 25 mm gauge length in compliance with ASTM B557-10 standard [18].

Table 1 Typical chemical composition (in wt%) of 6Si and Cu added 6Si samples from GD-OES analysis, elements having concentration less than 0.001 wt% are not shown here

Si	Fe	Cu	Ga	Ti	In	Mn	Ni	Ca	Sn	Mg	Zn	P
6.02	**1.97**	0.003	0.012	0.011	0.01	0.006	0.006	0.006	0.005	0.004	0.004	0.002
6.12	**1.96**	**2.11**	0.011	0.013	0.01	0.007	0.007	0.005	0.007	0.005	0.009	0.002
6.08	**2.01**	**4.02**	0.009	0.009	0.015	0.006	0.008	0.005	0.008	0.005	0.009	0.001

Results and Discussions

The calculated isopleth at 2 wt%Fe obtained from CALPHAD calculation is depicted in Fig. 1; where 6Si composition line is indicated. We note that though lever rule, in general, can not be applied in such isopleth, nevertheless it is helpful in determining the phases present at any given temperature and composition. Figure 2a shows solidification profiles of the base alloy as per Scheil and equilibrium solidification model. Figure 2b depicts the yield of β-phase during solidification at different level of Cu as per Scheil model; since most of the practical alloys follow Scheil model during solidification [19]. It is interesting to note that the calculated liquid phase fraction does not differ in an appreciable way between the two solidification models for a given alloy. The reason for such model invariant solidification is due to the fact, as can be seen from Fig. 1, that the liquid phase of the base alloy is in equilibrium with one of the intermetallic phases; namely, α-phase and β-phase (at lower temperature). Since, these intermetallic phases do not show appreciable range of solute solubility for either Si or Fe. Therefore, as solidification progresses only the fraction of intermetallic phase (β or α-phase) increases without any appreciable change in its composition; as exhibited by an equilibrium model or Scheil model. Therefore, the corresponding liquid phase fraction also remains model invariant at any given temperature. Only small deviation occurs between the two models due to the generation of pro-eutectic Al having appreciable solubility of Si. Thus, such variation is slightly more predominant where pro-eutectic Al is more, i.e. for compositions away from the eutectic composition.

Figure 3a is the as-cast microstructure of 6Si samples (as polished condition) in BSE mode where β-phase appears brighter due to the presence of heavy element like Fe.

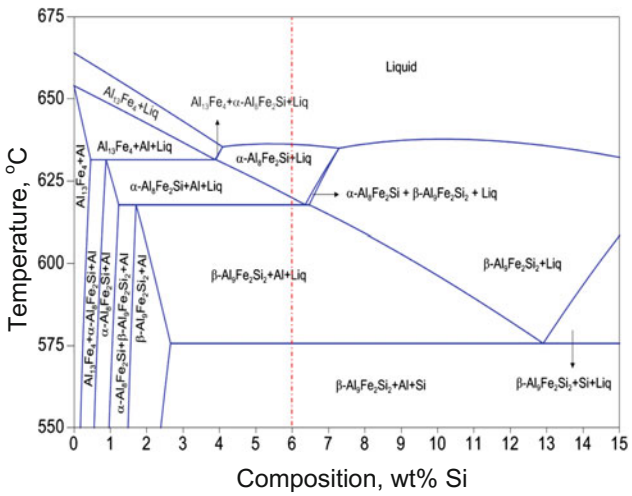

Fig. 1 Isopleth of Al–Fe–Si system sectioned at 2 wt%Fe, *red dashed lines* indicate 6 wt% and 10 wt%Si compositions

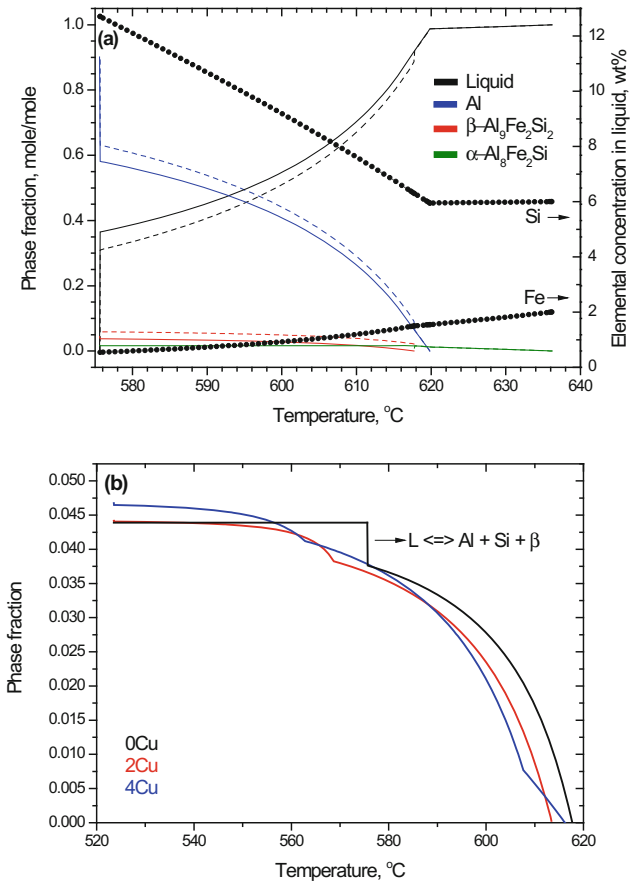

Fig. 2 **a** Simulation of solidification as per equilibrium model and Scheil model for 6Si alloy (0Cu or base alloy). *Solid line* indicates Scheil model of solidification whereas *dashed line* indicates lever rule method (equilibrium model). Symbol+line (*right hand axis*) are for the composition of the liquid phase. Note that liquid composition profile does not change much from equilibrium model to Scheil model. **b** Yield of β-phase as a function of temperature

Figure 3b is the as-cast microstructure with the addition of 4 wt%Cu with two noted features that are distinct from the base alloy; i.e. presence of eutectic Al_2Cu and absence of Al–Si eutectic. No noted difference was found between 2 wt%Cu and 4 wt%Cu except the lower amount of Al2Cu phase in the former.

Morphological Change of β-Phase

It is well known that solid-solid interfacial energy is always higher than the solid-liquid interfacial energy. Therefore, it is but natural to expect that the morphological change of the β-phase can minimise the interfacial energy, with suitable heat-treatment in solid-state. Accordingly, 6Si samples were isothermally held at 572 °C for 24 h. The idea behind this heat treatment is to go to a temperature as high as possible near to the eutectic point (575.7 °C) to facilitate faster diffusion of the chemical species and thereby facilitating faster change in the morphology of the β-phase. The microstructures of these samples are shown in Fig. 3c, d. Upon comparison with the as-cast sample (Fig. 3a) it becomes rather clear that the platelets of β-phase get refined by fragmentation. In fact, image analysis of 6Si sample reveals that the average aspect ratio of β-phase platelets reduces from 6.2 to 2.7 from the as-cast condition to the one isothermally held at 572 °C for 24 h as shown in Fig. 3c, d. Subsequent X-ray mapping clearly reveals that the grey-shaded rounded particles, almost obscured in the background (Al matrix), are nothing but Si particles; as evident from Fig. 4a, c. It is important to note that the Si particles also tend to be spheroidized during heat-treatment as indicated in these micrographs. Therefore, it could be considered that the as-cast microstructures of 6Si alloy are actually far from the equilibrium so long as the phase morphology is concerned. Similarly, a 24 h of soaking was given to 2 wt% Cu and 4 wt%Cu samples at 520 °C instead of 580 °C; owing to the lower solidus temperature of Cu added alloys. After this soaking treatment, microstructurally no difference was observed than that of base alloys, except for a small amount of Al_2Cu formation in 4 wt%Cu alloy. This indicates that most of the Cu goes into the solid solution.

It has also been thought to modify the morphology of the β-phase of base alloy by heat-treating just above the eutectic temperature, i.e. at 580 °C, but without inducing any segregation. Accordingly, only 2 h of soaking was given to 6Si samples at 580 °C. From Fig. 2a it could be seen that the phase fractions of the liquid phase is about 38% at 580 °C for 6Si alloy; however, no visual shape change was observed in 6Si sample after the heat-treatment. Microstructures for 6Si samples treated at 580 °C are presented in Fig. 3d. Based on the obtained results the following observations can be made:

(i) Change in morphology of β-phase is strongly dependent on the heat-treatment temperature. Aging above eutectic temperature (575.7 °C) causes faster growth of β-phase (in thickness) due to the faster diffusion in liquid phase [20]; whereas below 575.7 °C, growth process is slow and fragmentation across the length was observed.

(ii) Morphology of Si particles is also greatly dependent on heat-treatment temperature. Aging below eutectic temperature causes Si lamellae to become spheroidized, as shown in Fig. 4b. However, involvement of liquid phase (eutectic) during heat-treatment would give rise to zagged-blocky Si resembling to divorced eutectic morphology.

(iii) Addition of Cu tends to destroy the Al–Si eutectic structure rendering blocky shaped Si particles that become spheroidized upon isothermal soaking.

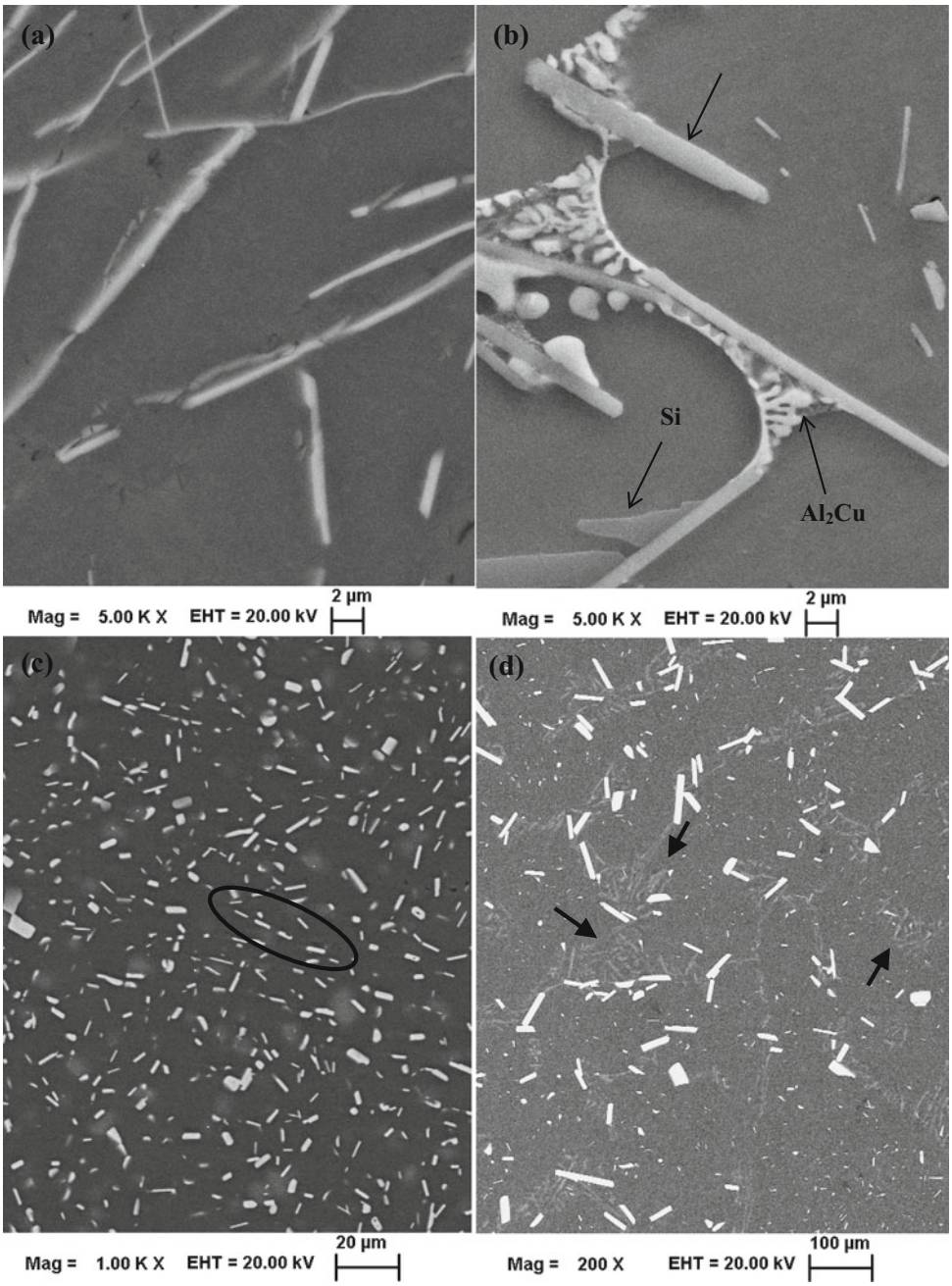

Fig. 3 BSE images in as-cast condition for **a** 6Si alloy and **b** with 4 wt%Cu addition; note the needle like white β-phase and Al_2Cu eutectic in (**b**). BSE micrographs of **c** 6Si samples held at 572 °C for 24 h reveals remarkable refinement of β-phase and fragmented yet aligned β-phase particles (*encircled*). **d** 6Si sample held at 580 °C for 2 h with coarse β-phase particles and needle like Si (*arrows*) grown within the liquid network

Mechanism of Morphological Change

We see from Fig. 3a, b that the β-phase platelets are of high aspect ratio; which is expected due to crystallographically anisotropic growth while precipitating from the liquid phase for faster accommodation of atoms across the liquid-beta interface during solidification. As a result, the as-cast microstructure is in morphologically metastable state due to high surface area of the primary β-phase platelets as indicated earlier. In order to minimize the surface energy two conditions must be satisfied simultaneously; microscopically the lowest energy crystallographic interface should prevail and macroscopically, surface area of β-phase platelet should be minimized [21]. Thus, during aging a dynamic equilibrium can be conceived, where atoms from β-phase diffused into matrix and precipitates again on the existing β-phase platelets towards satisfying these two conditions and thus minimizing the surface energy as well as the aspect ratio. Naturally, minimization of surface energy in this case would be a diffusion-controlled phenomenon and aging at higher temperature or involvement of a liquid phase would accelerate this process due to enhanced diffusivity. On the other hand, aging in solid-state condition

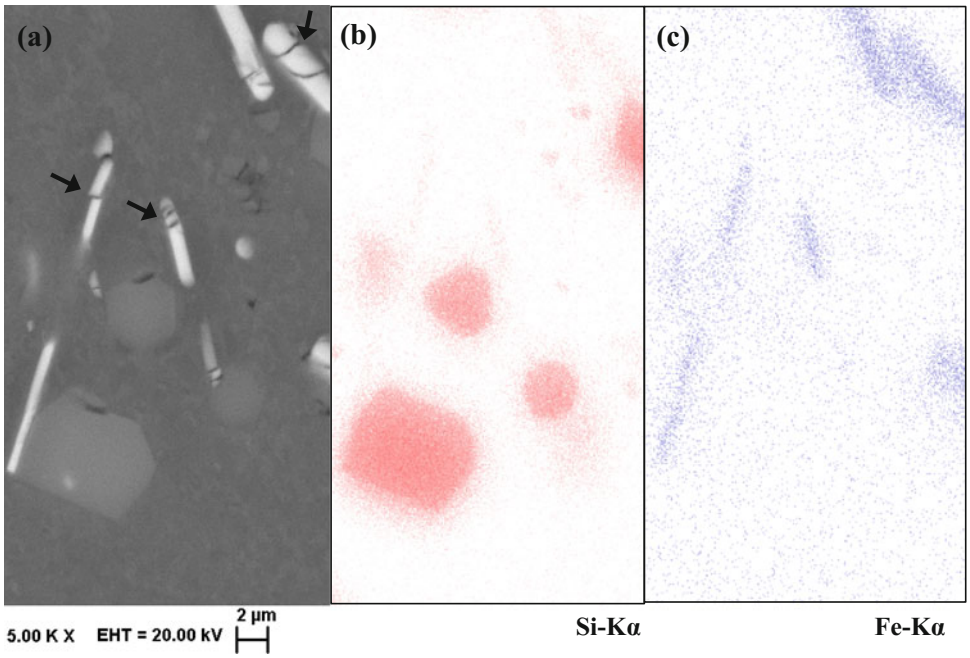

Fig. 4 **a** BSE micrographs of 6Si samples held at 572 °C for 24 h with x-ray mapping using **b** Si–K_α and **c** Fe–K_α. *Arrows* in (**c**) indicate the fragmented beta phase

would take longer time in order to achieve the low energy morphology due to lower diffusivity.

We note that β-phase always inherits longitudinal and transverse cracks as shown in Fig. 4a; which is studied in details and reported in the literature [22]. Such cracks provide additional high-energy surface area through which atomic diffusion could take place and eventually the platelets would appear in fragmented-yet-aligned morphology in the microstructure, as shown in Fig. 3c. In addition, the thickness of the fragmented platelets should increase upon isothermal treatment resulting in lower aspect ratio and round-edged particle as evident from Fig. 3c, d. The phenomenon of fragmentation and growth is depicted in Fig. 5 in a self-explained manner.

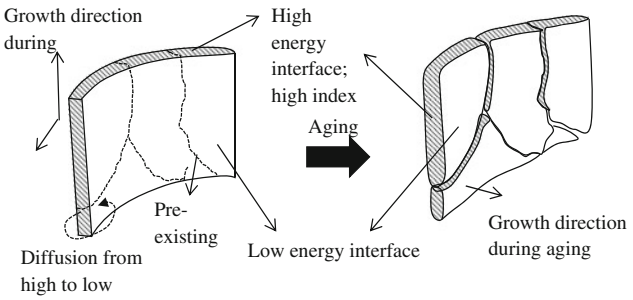

Fig. 5 Schematic growth model of primary β-phase platelet during solid-state aging. *Shaded surface* is the high-index crystallographic plane (for accommodating higher growth speed during solidification) representing high-energy interface and is perpendicular to the direction of solidification. Eventually, the β-phase would appear as fragmented-yet-aligned morphology with *rounded edge* and lower aspect ratio than their as-cast morphology

Tensile Properties

Based on the observations after aging, it was thought if a combined heat-treatment involving aging at 580 °C for 2 h followed by aging at 572 °C for 24 h would result in better mechanical properties. Accordingly, this heat-treatment was carried out for 6Si samples.

The tensile stress-strain curves of 6Si specimen with different heat-treated conditions are presented in Fig. 6a alongside with that of the as-cast specimen. From the figure, it is evident that the long-term soaking at 572 °C indeed causes improvement in ductility with loss in strength and yield strength. Tensile properties derived from the stress-strain curves are given in Table 2. This is also interesting to note the serrated plastic flow (Fig. 6a) in the spheroidized sample due to dynamic strain aging (DSA), which is also known as Portevin-LeChatelier effect (PLC effect). PLC effect in aluminium alloy due to dynamic strain aging is a known phenomenon and is reported in literature [23].

The correlations between the heat-treatment and corresponding morphology of the phases as well as the tensile properties appear to be straightforward. Improvement of the tensile properties strongly depends on the elimination of stress point rounded-off the existing eutectic Si phase and β-phase to a lesser extent causing improvement concentrating features (i.e. shape of existing β-phase or eutectic Si producing sharp

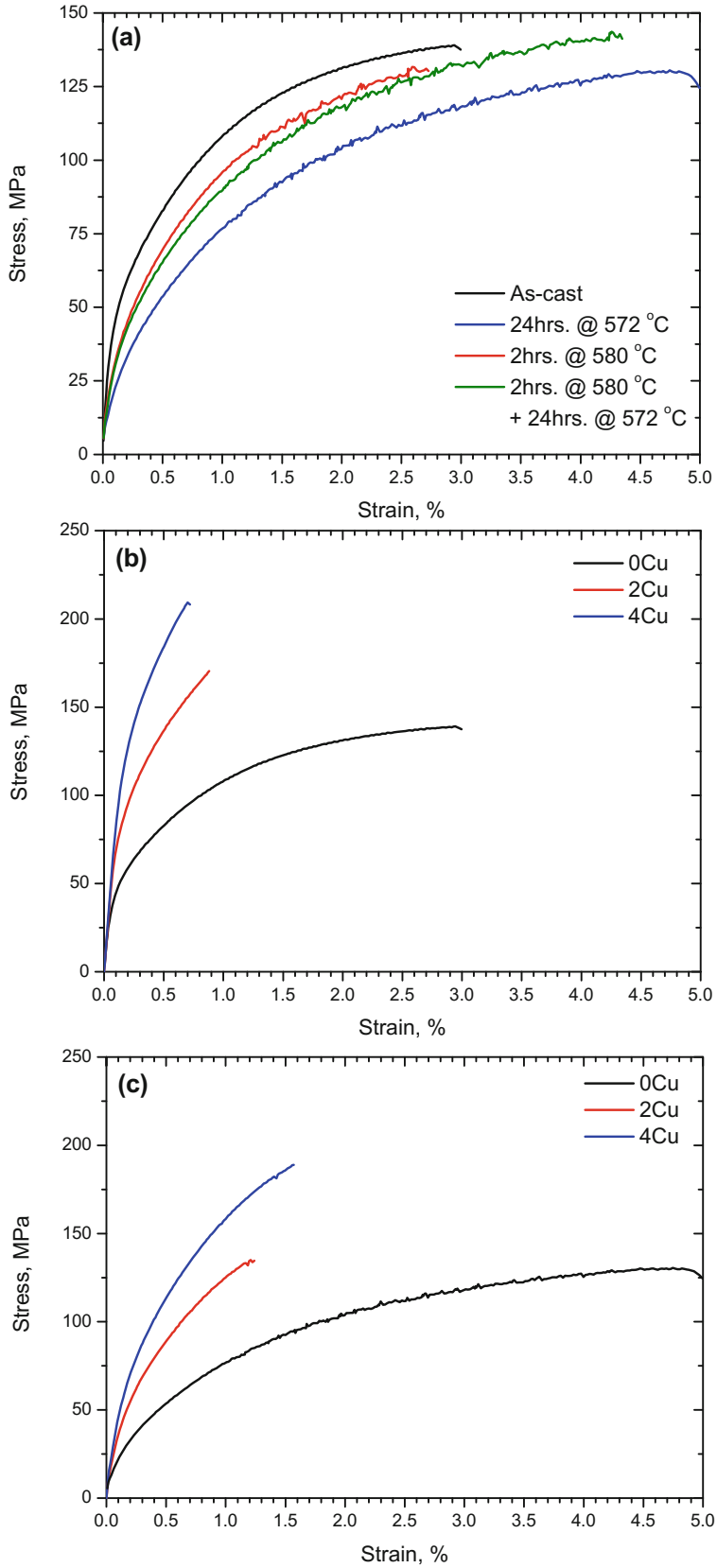

Fig. 6 **a** Comparative stress-strain curves of 6Si alloys with different heat-treatments. **b** Stress-strain curve in as-cast condition with different Cu level and **c** in solutionized condition for 24 h, at 572 °C for 0Cu and at 520 °C for 2Cu and 4Cu samples

Table 2 Typical tensile properties of 6Si alloy (with and without Cu addition) under different heat-treatment conditions

Sample, heat treatment ( )	Yield stress (0.2%) (MPa)	UTS (MPa)	Elongation (%)
0Cu, as-cast	70	139.1	2.6
2Cu, as-cast	124.1	170.4	0.6
4Cu, as-cast	173.8	209.3	0.4
0Cu, 24 h @ 572 °C	59.8	130.4	3.9
2Cu, 24 h @ 520 °C	81.1	134.6	0.9
4Cu, 24 h @ 520 °C	107.8	188.8	1.1
0Cu, 2 h @ 580 °C	66.5	131.6	2.2
0Cu, 2 h @ 580 °C then 24 h @ 572 °C	61.8	143.6	3.8

corners) in high Fe bearing Al–Si alloy. Isothermal treatment for prolonged time below eutectic in ductility in all alloys. However, grain growth in base alloy causes reduction in 0.2% offset yield strength and UTS. Addition of Cu was aimed to improve the strength in as-cast condition and even after the long-term isothermal spheroidizing treatment, as evident from Fig. 6b, c. It is interesting to note that holding for a shorter period slightly above eutectic temperature does not exhibit better tensile properties than that of as-cast structure despite the fact that β-phase grows with lowering in particle count (Ostwald ripening) and as a result many of the stress raisers (sharp corners) are eliminated. This could be explained by considering the fact that upon solidification from 680 °C, the Si morphology gives rise to zagged flaky shape with sharp corners (Fig. 3d) and at the same time, average grain size increases, which reduces both ductility and strength. However, the best result is obtained when the same sample is again subjected to solid-state aging below eutectic temperature causing rounding off the edges of eutectic Si along with the rounded β-phase. Addition of Cu increases both YS and UTS, albeit with a reduction in ductility. At this point the best possible combination of tensile property could be achieved in 4 wt%Cu sample with isothermal treatment at 520 °C. We emphasize that there is a large scope of optimization in terms of alloy addition, spheroidizing temperature and soaking time in order to obtain the best possible combination of the tensile properties.

Conclusions

From the foregoing discussion the following concluding points could be drawn:

(i) Morphological change of β-phase (via suitable heat-treatment) in Al–6 wt%Si–2 wt%Fe alloy with or without Cu addition was studied to counteract the detrimental effect of Fe content.
(ii) Fragmentation theory has been proposed as the chief mechanism for the refinement of the β-phase upon solid-state spheroidizing treatment based on the experimental evidences; this also improves tensile properties.
(iii) Isothermal treatment above and below eutectic point in 6Si alloy spheroidizes both β-phase and Si particles, causing further improvement in ductility and ductility.
(iv) Addition of Cu increases the strength with a loss in ductility, it also destroys the Al–Si eutectic structure and Si appears as blocky particles.

Acknowledgements The authors acknowledge that the present work has been carried out under the aegis of Marie Sklodowska Curie Individual Fellowship (MSCA-IF-2014), European Commission (EU project no. 656943).

References

1. J.A.S. Green (ed.), *Aluminum recycling and processing for energy conservation and sustainability* (ASM International, USA, 2007)
2. C. Schmitz (ed.), *Handbook of aluminium recycling* (Vulkan Verlag, Germany, 2006)
3. G. Gaustad, E. Olivetti, R. Kirchain, Resour. Conserv. Recycl. **58**, 79 (2012)
4. V.G. Rivlin, G.V. Raynor, Int. Met. Rev. **26**, 133 (1981)
5. G. Ghosh, in *Ternary Alloys*, vol. 5, ed. by G. Petzow, G. Effenberg (VCH Publishers, Germany, (1992)) p. 394
6. N. Krendelsberger, F. Weitzer, J.C. Schuster, Met. Mat. Trans. A **38A**, 1681 (2007)
7. M.C.J. Marker, B. Skolyszewska-Kühberger, H.S. Effenberger, C. Schmetterer, K.W. Richter, Intermetallics **19**, 1919 (2011)
8. A. Gorny, J. Manickaraj, Z. Cai, S. Shankar, J. Alloy Com. **577**, 103 (2013)
9. C.B. Basak, N. Haribabu, Mat. Design **108**, 277 (2016)
10. J.A. Taylor, Proc. Mat. Sci. **1**, 19 (2012)
11. C.M. Dinnis, J.A. Taylor, A.K. Dahle, Scripta Mater. **53**, 955 (2005)
12. S.G. Shabestari, Mat. Sci. Eng. A **383**, 289 (2004)
13. E. Taghaddos, M.M. Hejazi, R. Taghiabadi, S.G. Shabestari, J. Alloy. Comp. **468**, 539 (2009)

14. N.A. Belov, A.A. Aksenov, D.G. Eskin, *Iron in aluminium alloys: impurity and alloying element* (Taylor & Francis Inc., New York, 2002)
15. H.L. de Moraes, J.R. de Oliveira, D.C.R. Espinosa, J.A.S. Tenorio, Mater. Tran. **47**(7), 1731 (2006)
16. S.L. Chen, F. Zhang, F.Y. Xie, S. Daniel, X.Y. Yan, Y.A. Chang, R. Schmid-Fetzer, W.A. Oates, JOM **55**(12), 48 (2003)
17. W.S. Rasband, in *ImageJ*, (U. S. National Institutes of Health, Bethesda, Maryland, USA, 1997–2015), http://imagej.nih.gov/ij/
18. ASTM B557-10 Standard Test Methods for Tension Testing wrought and cast aluminium and magnesium alloy product (2015), ASTM International, West Conshohocken, PA. www.astm.org
19. C.B. Basak, M. Krishnan, Phil. Mag. Lett. **95**, 376 (2015)
20. J. Wang, P.D. Lee, R.W. Hamilton, M. Li, J. Allison, Scripta Mat. **60**(7), 516 (2009)
21. C.B. Basak, J. Nucl. Mat. **416**(3), 280 (2011)
22. X. Cao, J. Campbell, Mater. Tran. **47**(5), 1303 (2006)
23. K. Peng, W. Chen, K. Qian, Mat. Sci. Eng. A **415**(1–2), 53 (2006)